

Full Length Article

Reaction molecular dynamics simulation of kerogen hydrogenation catalysis in marine deep shale



Guili Ma ^{a,b}, Junqing Chen ^{a,b,*}, Changtao Yue ^{a,b,*}, Yue Ma ^{a,b}, Lu Gong ^{a,b}, Yuying Wang ^{a,b}, Fujie Jiang ^{b,c}, Hong Pang ^c, Xinyi Niu ^{a,b}

^a College of Science, China University of Petroleum (Beijing), No. 18 Fuxue Rd., Changping District, Beijing 102249, PR China

^b Basic Research Center for Energy Interdisciplinary, College of Science, China University of Petroleum(Beijing), No. 18 Fuxue Rd., Changping District, Beijing 102249, PR China

^c College of Geosciences, China University of Petroleum (Beijing), No. 18 Fuxue Rd., Changping District, Beijing 102249, PR China

ARTICLE INFO

ABSTRACT

Keywords:

Over-mature shale
Kerogen
Hydrocarbon generation mechanism
ReaxFF molecular dynamics
Hydrogenation catalysis
Deep-Ultra deep

Studying the activation mechanism of over-mature kerogen for hydrocarbon generation is crucially important for the deep-ultra deep oil and gas exploration and development. Recent research revealed that the presence of external hydrogen sources could reactivate the complex hydrocarbon generation processes of kerogen, which is different with traditional theory. However, the underlying mechanisms are not entirely clear. In this paper, reactive molecular dynamics (RMD) with reactive force field (ReaxFF) was used to simulate the pyrolysis of hydrocarbons in an aqueous mixed-system model of over-mature kerogen from the Longmaxi Formation in the Sichuan Basin of China. The distribution characteristics of the products of natural gas (C₁–C₄), light oil (C₅–C₁₃), heavy oil (C₁₄–C₃₉), coke (C₄₀₊) were analyzed to construct the reaction pathways of the kerogen conversion. The simulation results showed that adding water as catalyst and H agent, kerogen could be reactivated to generate hydrocarbons when the reaction temperature increased from 1000 to 3000 K. The total rate of hydrocarbon generation could reach up to 22.28 % and break through the hydrocarbon generation dead line of traditional hydrocarbon generation models. In the high temperature stage at 2500 K, heavy oil molecules underwent secondary cracking into smaller oil and gas components, leading to a decrease in the yield of heavy oil. At the initial stage of the extended reaction time at 2500 K, increasing the reaction time by 1 time could significantly promote the generation of oil and gas productions by 3.65 times. While further increasing reaction time by 1 time has a relatively minor impact on oil and gas productions by 0.45 times. During the pyrolysis process, kerogen molecules broke in the following order based on bond energies, the C_{al}-S bond, C_{ar}-C_{al}-O bond, C_{al}-C_{al} bond, C_{al}-C_{al}-O bond, C_{ar}-C_{al} bond and C_{al}-H bond. Meanwhile, a special reaction pathway of hydrolytic disproportionation and hydrocarbon generation was revealed under the condition of hydrogen supply of H₂O. The research results are of great significance to reveal the mechanism of hydrocarbon generation by pyrolysis of over-mature kerogen, to guide the evaluation of deep-ultra deep hydrocarbon resources, and to optimize the selection of exploration deserts.

1. Introduction

Once discovered, oil and gas have become the most important energy and material sources in every country on earth. During the development of modernization and industrialization processes of our society, the oil and gas demand has been increased rapidly, especially for China. Meanwhile, it is noted that traditional oil and gas resources have already been unable to fulfill current demand, making it particularly important

to search for new sources of oil and gas. Presently, the oil and gas exploration in China has successively stepped into the ultra-deep strata (where the depth of the strata is beyond 6,000 m), and a series of large and super-large oil and gas fields have been discovered distinctly demonstrating the vast exploration potential of the ultra-deep sedimentary basins in China [1–6]. Investigating the physical and chemical properties and behaviors of shale in ultra-deep strata gas and oil reservoir not only provides the fundamental understandings on the

* Corresponding authors at: College of Science, China University of Petroleum (Beijing), No. 18 Fuxue Rd., Changping District, Beijing 102249, PR China.
E-mail addresses: cjq7745@163.com (J. Chen), yuect@cup.edu.cn (C. Yue).

generation and expulsion of hydrocarbons, but also serves as the valuable reference for oil and gas exploration.

Numerous research efforts have been focused on the hydrocarbon generation mechanism of source rocks using different experiment designs. Among them, pyrolysis hydrocarbon generation experiments are important methods to reveal the mechanisms of hydrocarbon generation and transformation behaviors of organic matter, and evaluate the potential of hydrocarbon generation [7,8]. Tissot et al. have simulated the long-term thermal evolution and hydrocarbon generation process of organic matter from source rocks by means of rapid temperature rise [9]. They found that the negative influence of insufficient time on the thermal evolution processes of organic matter can be compensated by high temperature, which could vastly promote the production efficiency of hydrocarbons. Meanwhile, the mechanisms and characteristics of hydrocarbon generation of kerogen were studied mainly through simulation experiments and calculation of hydrocarbon generation kinetics [10–14]. However, such work was unable to reproduce the reaction process and reaction pathways.

In recent years, ReaxFF MD simulations have been successfully applied to the investigation of primary reaction mechanisms and kinetics associated with pyrolysis [15–18], combustion [19,20], and heteroatom conversion and migration processes [21–24] of fossil fuels (coal, oil shale, etc.). In addition, ReaxFF MD was also widely used in kerogen pyrolysis simulation to reveal the reaction mechanism of kerogen pyrolysis at the molecular scale [25–30]. Zhang et al. employed the ReaxFF MD simulation approach to investigate the product distribution and organic sulfur removal in the course of direct pyrolysis and hydropyrolysis of kerogen within oil shale. In contrast to direct pyrolysis, hydropyrolysis was capable of supplying a greater number of H radicals to engage in the reaction, thereby facilitating the pyrolysis reaction of kerogen [31]. Zhao et al. carried out ReaxFF MD simulation on the Fushun oil shale kerogen model, uncovering three mechanisms of H₂ formation under superheated steam: one was the formation of H₂ from two hydrogen radicals of kerogen, the other was that two hydrogen radicals from superheated steam and kerogen form H₂, and another originated from two hydrogen radicals in superheated steam forming H₂ [32]. ReaxFF MD was indeed a potent method that could effectively trace the chemical reaction paths and elucidate the mechanism of hydrocarbon generation from kerogen.

Shale is mainly composed of organic matter and inorganic minerals, and the main component of organic matter is kerogen, which can be converted into oil and natural gas via pyrolysis processes [33]. Kerogen in deep-ultra deep shale has largely evolved to produce hydrocarbons, resulting in a lack of hydrogen and an H/C atomic ratio < 1.0. According to the classical organic hydrocarbon generation model, the hydrocarbon generation potential of high-over-mature kerogen has been nearly exhausted due to the restriction of hydrogen content in the kerogen [34]. Seewald proposed that water could be used as an external hydrogen source to join the reaction of kerogen to generate natural gas in the deep basin at the highly evolved stage, while the traditional hydrocarbon generation model underestimated the hydrocarbon generation potential of organic matter at the highly evolved stage of kerogen [35]. Jia and Zhang suggest that high temperature conditions and deep fracture cause the existence of a variety of highly reactive hydrogen-rich fluids such as water in rocks (pore water, mineral structure water and hot water from deep sources, etc.), water–rock reaction or H₂ from deep sources. These hydrogen-rich fluids can serve as an important external hydrogen source for hydrocarbon generation by organic matter under high temperature conditions [5]. However, the hydrocarbon generation behaviors and mechanisms of highly over-matured kerogen with water as the external hydrogen source are still not entirely clear.

In this paper, the hydrocarbon regeneration characteristics, product distributions and reaction processes of over-matured kerogen from Longmaxi Formation of the Sichuan Basin were investigated using the ReaxFF MD method. The results can provide theoretical basis for the evaluation of deep-ultra deep oil and gas resources and the selection of

favorable exploration zones.

2. Material and methods

2.1. Selection of typical deep-ultra deep kerogen model

The maximum burial depth of Longmaxi Formation shale gas reservoirs in Sichuan Basin and the mid-shallow layers are 6000 ~ 7000 m. The maximum burial depth of the Lower Cambrian shale in the Sichuan Basin and its periphery exceeds 8000 ~ 10,000 m. At present, the development and production of medium and shallow shale gas reservoirs have reached as far as 3500 m [36]. In this paper, the typical deep-ultra deep shale kerogen macromolecular model was selected from the average molecular structure model of the shale kerogen of Longmaxi Formation [37]. The vitrinite reflectance (Ro) of the shale kerogen of Longmaxi Formation is about 2.8 %, which is over-matured and belongs to type II kerogen.

2.2. Establishment and optimization of 3D molecular configuration

Liu et al. [37] have characterized the over-matured shale type II kerogen ($C_{205}H_{158}O_{19}N_4S_4$) in Longmaxi Formation, Sichuan Basin using isothermal adsorption, XRD, FTIR and ¹³C NMR to analyze and construct the basic structure of kerogen. The specific molecular chemical structure is shown in Fig. 1.

In order to construct the molecular structure model of kerogen, the Forcite module of Materials Studio software was used to optimize the structure under the condition of minimum molecular energy. The target and precision parameters of the Forcite module were set as Geometry optimization and Fine, respectively, and the Dreiding force field was used. The maximum number of calculation cycles was set to be 50,000. The charge distribution was QEq, the van der Waals forces and electrostatic effects to Atom based were applied. The three-dimensional molecular structure model and energy trend diagram of kerogen optimized by MS software are shown in Fig. 2. After optimization, the energy of the organic macromolecule model reached its minimum and formed a stable configuration.

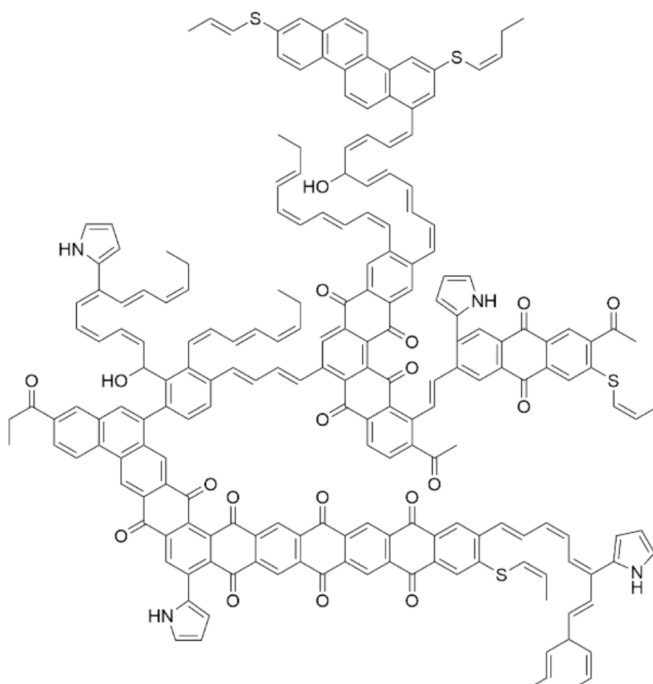


Fig. 1. Molecular structure model of Longmaxi Formation shale kerogen.

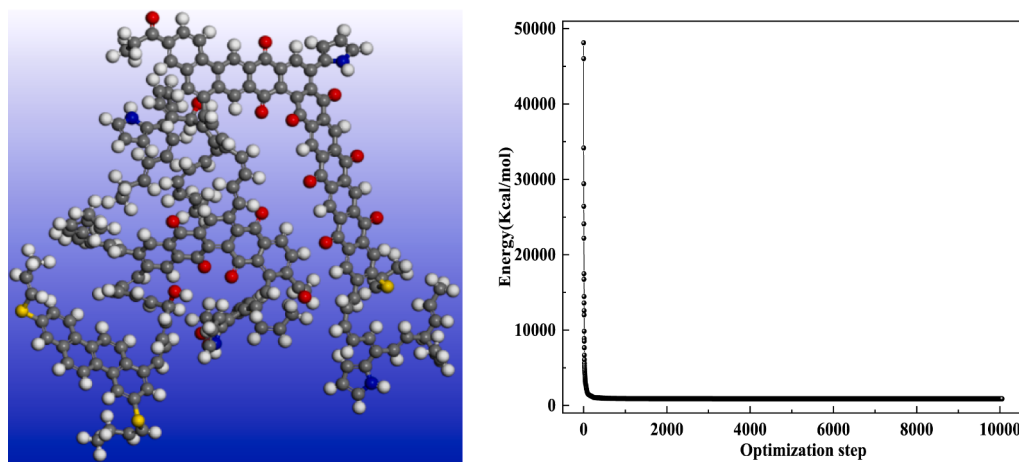


Fig. 2. Three-dimensional structure model(left) and optimization energy of kerogen molecule(right).

2.3. Principles of molecular dynamics of reactions

Classical molecular dynamics methods are able to conduct the simulation calculation with large systems, but they cannot accurately describe chemical reaction processes. By combining the advantages of quantum mechanics and classical molecular dynamics, ReaxFF MD provides detailed information on the forming and breaking behaviors of chemical bonds in a complex reaction system [38]. ReaxFF is a non-reactive force field that utilizes the bond order principle to simulate the chemical and physical interactions of atoms and molecules in complex reaction systems. Similar to an empirical non-reactive force field, a reactive force field divides the system energy into distinct partial energies as in Eq. (1).

$$E_{\text{system}} = E_{\text{bond}} + E_{\text{atom}} + E_{\text{lp}} + E_{\text{val}} + E_{\text{coa}} + E_{\text{hb}} + E_{\text{tors}} + E_{\text{conj}} + E_{\text{coulomb}} + E_{\text{vdw}} + E_{\text{charge}} \quad (1)$$

where E_{system} is the total energy of the system, E_{bond} is the bond energy, E_{atom} is over + under-coordinated energy, E_{lp} is the lone pair electron energy, E_{coa} is the angular conjugation energy, E_{val} is valence Angle energy, E_{tors} is torsion Angle energy, E_{hb} is hydrogen bond energy, E_{coulomb} is the coulomb energy, E_{conj} is the conjugation energy, E_{vdw} is van der Waals energy, and E_{charge} is the charge polarization energy.

2.4. Reaction molecular dynamics simulation process

The molecular dynamics simulation process of kerogen molecular reaction using AMS platform mainly includes four steps, that is structure optimization, hybrid system creation, compression and relaxation, and molecular reaction dynamics simulation (Fig. 3).

Firstly, the structure of kerogen macromolecules and water molecules was preliminarily optimized by UFF force field, and then Geometry Optimization was carried out. The length of C-S bond after UFF force field Optimization and Geometry Optimization was 1.61 Å and 1.88 Å.

The second step was to create a mixed system containing water and kerogen molecules. Considering the geological conditions and the assumption that the amount of water should not be the limiting factor for the reaction [39,40], 20 large molecules of kerogen in the Longmaxi Formation shale and 2000 water molecules were included in the simulation system. The lattice constant of 90 Å was constructed to make its

density low (0.2236 g/cm³) and the mixture system was generated.

The third step was compression and relaxation. The dynamic parameters related to relaxation were set and the force field was selected as "HCONSB". The total number of steps was 100,000, the time step was 0.25 fs, the temperature was 100 K, the number of compression steps was 80,000, the lattice constant was 49 Å, and the remaining 20,000 steps were relaxation at constant volume. The state of the system before and after relaxation compression is shown in Fig. 4. In the process of relaxation compression, the energy first decreases rapidly and then becomes stable, and the change curve is shown in Fig. 5. After relaxation compression, the energy of the system becomes lower and the system becomes more stable. The compressed density is 1.386 g/cm³, which is consistent with the reasonable density of kerogen molecules 1.1–1.4 g/cm³[9].

Finally, the Molecular Dynamics of kerogen hydrocarbon generation was calculated. The Molecular Dynamics task under the ReaxFF module of AMS software was selected, the force field was selected as "HCONSB", and the time step was 0.25 fs. The molecular dynamics simulation of the reaction mainly included reaction temperature effect and reaction time effect. The target reaction temperature was set as 1000 K, 1500 K, 2000 K, 2500 K and 3000 K, and the total reaction steps were set as 1 million steps. The effect of reaction time on hydrocarbon generation products at the same reaction temperature was studied. The target reaction temperature was 2500 K and the maximum reaction time was set to 1.6 million steps (400 ps). The temperature settings for the pyrolysis hydrocarbon thermostat were designed to examine the effects of both reaction temperature and reaction time. The temperature settings were detailed as follows. A constant temperature state of 50,000 steps was maintained at 100 K. Subsequently, it required 350,000 steps to reach the reaction temperature with a certain rate of increment. Then, a 600,000 steps constant temperature was sustained at the reaction temperature. Especially, when the reaction temperature was 2500 K, it was prolonged by maintaining a 600,000 steps constant temperature at the same level.

3. Results and discussion

3.1. Influence of reaction temperature

Based on the number of carbon atoms, the molecules of hydrocarbon

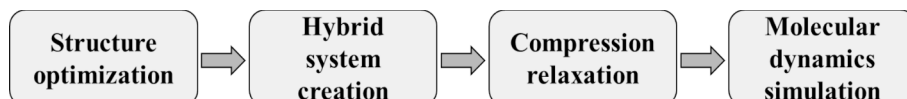


Fig. 3. Flow chart of reaction molecular dynamics simulation.

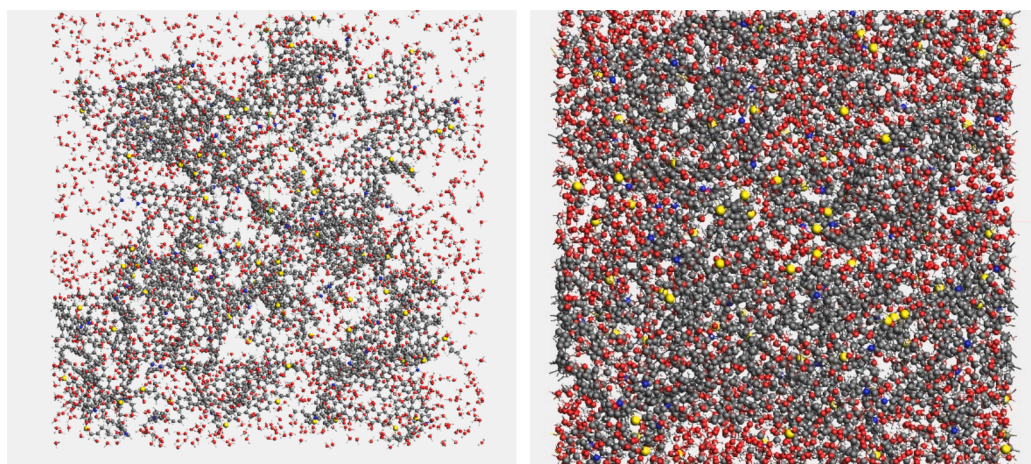


Fig. 4. Reaction system before (left) and after (right) relaxation compression.

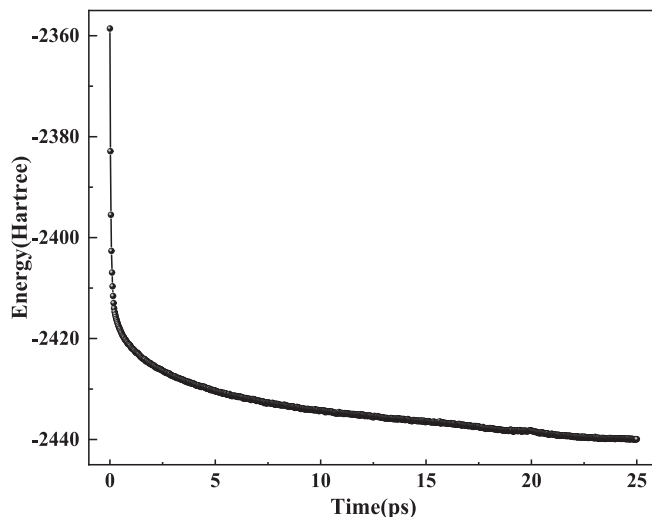


Fig. 5. Energy change curve during relaxation compression.

products can be classified into four categories [21,30,41], which are nature gas (C_1-C_4), light oil (C_5-C_{13}), heavy oil ($C_{14}-C_{39}$), and coke (C_{40+}). As shown in Fig. 6, the reaction temperature is an important factor affecting the product distribution during pyrolysis processes. As the reaction temperature increases, the small molecule compounds continue to increase, with high temperature favoring the generation of natural gas (C_1-C_4) and low temperature favoring the formation of larger molecules.

As shown in Fig. 6 (a), with the increasing of reaction temperature, the average molecular weight of molecules in the system exhibits an increasing trend firstly, but followed with a decreasing behavior. The maximum value has been reached at around 1500 K. This phenomenon is due to that kerogen molecules mainly undergo decarboxylation and dehydration reactions at low temperature, resulting in the formation of small molecular compounds. However, when the temperature increases, kerogen molecules prefer to undergo polymerization processes and generate organic macro-molecules with higher molecular weight. At higher temperature, the C–C and C–H bonds with large bond energy in kerogen molecules could break to form shale oil with relatively small molecular weight. Hence, the average molecular weight of substances in the system slowly decreases again.

Fig. 6 (b) and Fig. 6 (c) show that in the temperature range of 1000 to 3000 K, coke gradually decreases with the increasing of reaction temperature, whilst natural gas and light oil gradually increase. Heavy oil

exhibits the increase–decrease behavior, reaching its highest value at the temperature of 2000 K. This simulated pyrolysis product results are consistent with the reported experimental results [42]. Namely, the pyrolysis gas production increased monotonically with the increase of temperature. The heavy oil production initially increased and then decreased with the increase of temperature, which was due to the secondary cracking reaction at high temperature.

The gases in the pyrolysis products of kerogen molecules mainly include non-hydrocarbon gases (H_2O , CO_2 , H_2S , H_2 , NH_3 , etc.) and hydrocarbon gases (C_1-C_4 gases). With the increase of reaction temperature, the content of non-hydrocarbon gases such as H_2 , CO_2 , NH_3 , etc. was increased in Fig. 6 (d). Among them, the CO_2 content has the most significant increment, indicating that the high temperature promotes the generation of CO_2 . H_2S gas content firstly increased and then decreased, reaching its maximum at the temperature of around 2500 K, indicating the favorable temperature for the generation of H_2S . As to hydrocarbon gases in Fig. 6 (e), the contents of CH_4 , C_2H_2 and C_2H_4 were increased along with the increasing temperature. Nevertheless, C_3H_6 and C_4H_8 contents were firstly increased and then decreased, indicating that high temperature was beneficial for the generation of small molecule components.

The liquid products in the pyrolysis products of kerogen molecules mainly include light oil (C_5-C_{13}) and heavy oil ($C_{14}-C_{39}$). As the reaction temperature increases, the total amount of the liquid products gradually increases, as shown in Fig. 6(f). Thereinto, the light oil yield gradually increases, whereas the heavy oil yield first increases and then decreases in Fig. 6(c).

Statistical analysis results of the molecular number of the simulated reaction products in Fig. 7 (a) shown that as the reaction temperature increases, the molecular species of pyrolysis products gradually increased from 114 substances in 1000 K system to 558 substances in 3000 K system. Meanwhile, the number of molecules in the reaction system first decreases and then increases at each temperature point. Above phenomenon is consistent with the average molecular weight of the products in Fig. 6(a), which indicates that the active chemical bonds in kerogen molecules are partially cracked and broken at low temperature to generate small molecular compounds. Increasing reaction temperature could lead to the polymerization reaction among kerogen molecules to form organic molecules with higher molecular weight. At temperature of 2500 K, the stable chemical bonds in kerogen molecules are also broken, giving rise to the generation of oil and gas components with relatively small molecular weight.

The pyrolysis products of kerogen at high temperature show the significantly increasing in the number of small and medium molecular compounds in Fig. 7 (b) to Fig. 7 (h), such as H_2O , CH_4 , C_2H_6 , H_2 , CO_2 , H_2S and NH_3 , which are not generated below 2000 K. Besides, the

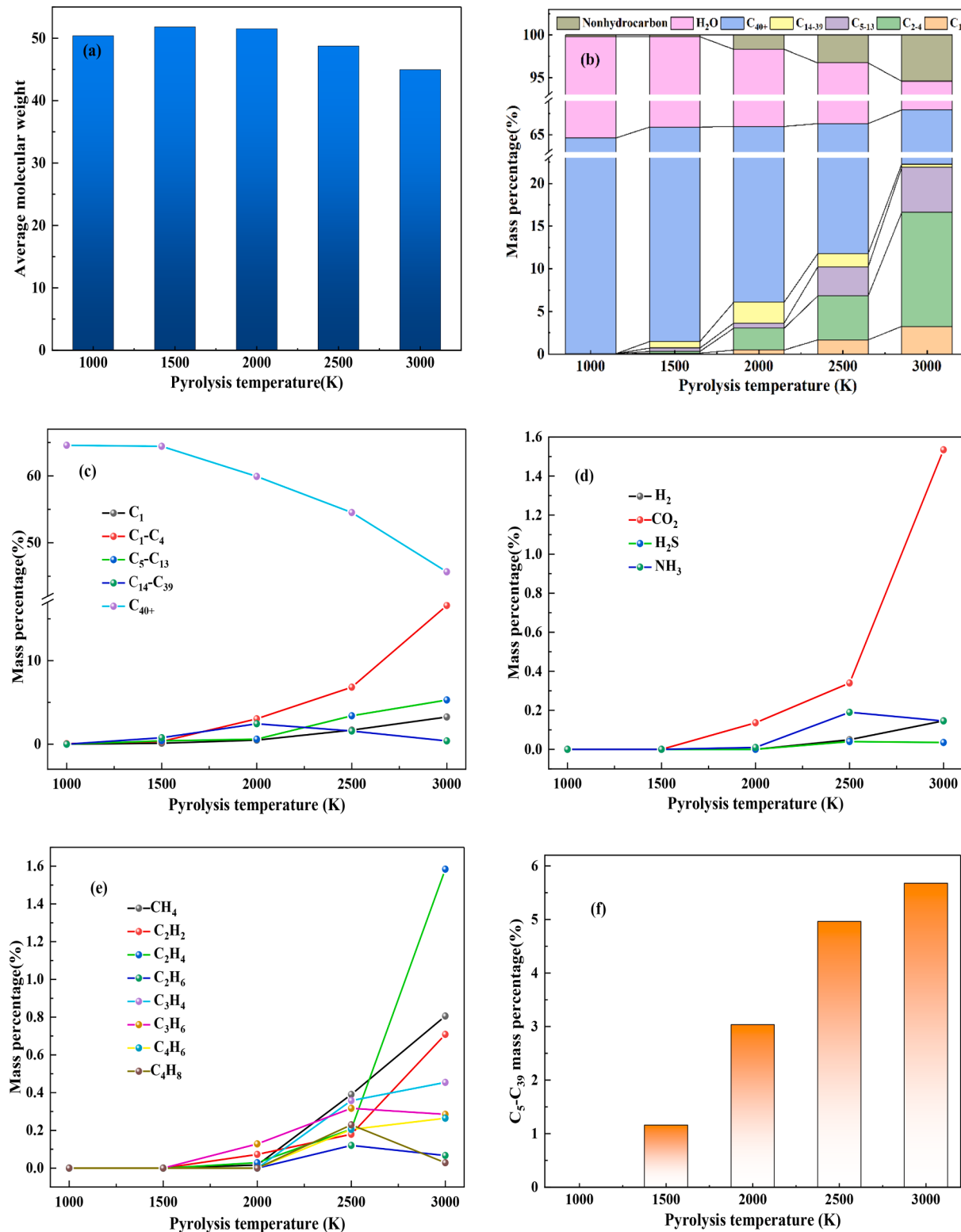


Fig. 6. Composition evolutions of pyrolysis products with reaction temperatures: (a) average molecular weight of products, (b) all pyrolysis products, (c) hydrocarbon products, (d) mainly non-hydrocarbon products, (e) gaseous hydrocarbon products and (f) liquid hydrocarbon products.

number of H₂O molecules in the system gradually decreases, as they are decomposed into H and OH free radicals at high temperature (Fig. 7 (i) and Fig. 7 (j)), which serve as the hydrogen source for the pyrolysis reaction system of kerogen. This is conducive to the pyrolysis of kerogen into oil and gas. As shown in Fig. 7 (j), H free radicals do not appear at low temperatures of 1000 K and 2000 K, because the breaking of

chemical bonds during kerogen pyrolysis basically complies with the principle of minimum bond dissociation energies (BDEs)[25,26,43]. The energy changing tendency is C-S bond < C-N bond < C-O bond < C-C bond < C-H bond < C=C bond [43]. C-H is not easy to form H radicals because of the large bond energy; meanwhile, H radicals are more active and likely to react to form other compounds[25].

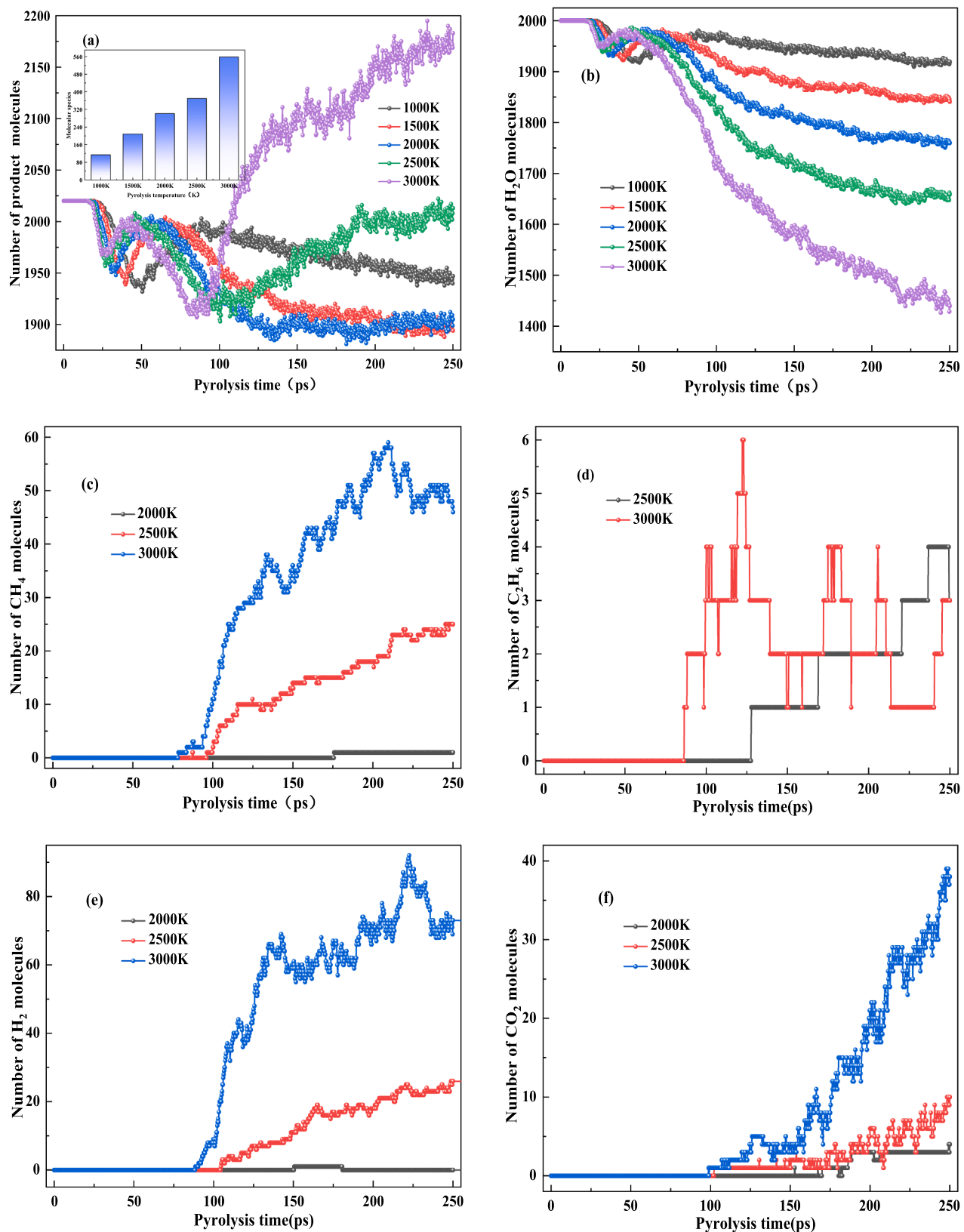


Fig. 7. Molecular number evolutions of pyrolysis products with the reaction time: (a) Number of product molecules with species, (b) H_2O , (c) CH_4 , (d) C_2H_6 , (e) H_2 , (f) CO_2 , (g) H_2S , (h) NH_3 , (i) HO and (j) H .

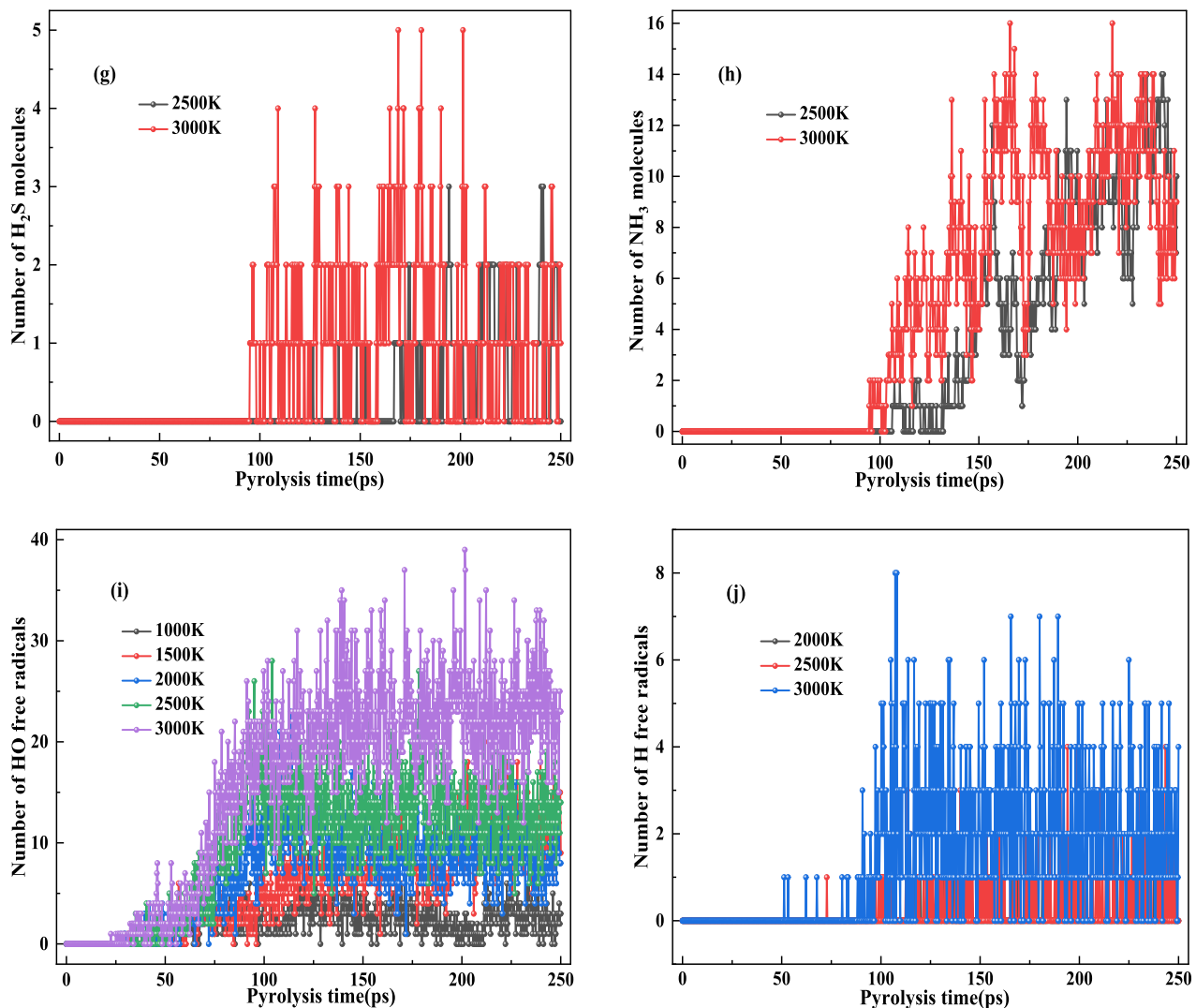


Fig. 7. (continued).

3.2. Influence of reaction time

Except for reaction temperature, the pyrolysis reaction time is also an important influence factor in the distribution of pyrolysis products as well as the evolutionary pattern. In this part, the reaction time was extended to 400 ps when the reaction temperature was kept at 2500 K. The variation of pyrolysis products with reaction time is shown in Fig. 8 (a).

As shown in Fig. 8(b), the gas and liquid gradually increase and eventually remain constant with the reaction time increases, while the coke decreases and eventually stays unchanged. Meanwhile, the effect of reaction time on the process of hydrocarbon generation exhibits a three-stage pattern. During the initial stage from 100 to 200 ps, the yield of oil and gas increases from 2.78 to 12.96 %, representing an increase of 3.65 times. During the middle stage from 200 to 300 ps, the yield of oil and gas rises from 12.96 to 16.24 %. During the later stage from 300 to 400 ps, the yield of oil and gas ascends only from 16.24 to 18.76 %.

Except for hydrocarbon products, the production of non-hydrocarbon gases including H_2 , CO_2 and H_2S also increase as the time has been prolonged in Fig. 8(c). Among them, the increase of CO_2 is the fastest, indicating that the increase of reaction time was suitable for the generation of CO_2 . As shown in Fig. 8(d), CH_4 , C_2H_4 and C_2H_6 increased, meanwhile C_2H_2 , C_4H_6 and C_4H_8 increased first and then decreased, indicating that increasing the reaction time was suitable for

the formation of smaller molecular components. With the increase of reaction time in Fig. 8(a) and Fig. 8(e), the production of light oil and heavy oil gradually increased, but the increase was not large, and finally tended to be stable. At the same time, the liquid hydrocarbon yield also has a similar trend of light oil and heavy oil.

3.3. Analysis of pyrolysis reaction mechanism

ChemTrayze code was used to analyze trajectory files simulated by ReaxFF MD under different pyrolysis conditions. Combined with previous research results [44–47], the distribution and characteristics of bond energy of major chemical bonds in kerogen (Table 1) [46] were summarized and categorized. Subsequently, the results inferred the decomposition steps of kerogen molecular model in the heating reaction process as follows:

Firstly, the three-dimensional structure decomposition process of kerogen generates a large number of molecular compounds, where the preferred bond cleavage sites are the C–C bonds connected to carbonyl carbon atoms, carboxyl groups, C–N bonds, and C–S bonds on fatty carbons. Kerogen molecules and molecular compounds continue to decompose and produce a large number of free radicals and molecular fragments. The bond cleavage sites are the C–C and C–O bonds in the aliphatic ring or aliphatic chain, the C–C bonds in branched structures, and the β -position C–C and C–N bonds connected to aromatic carbon

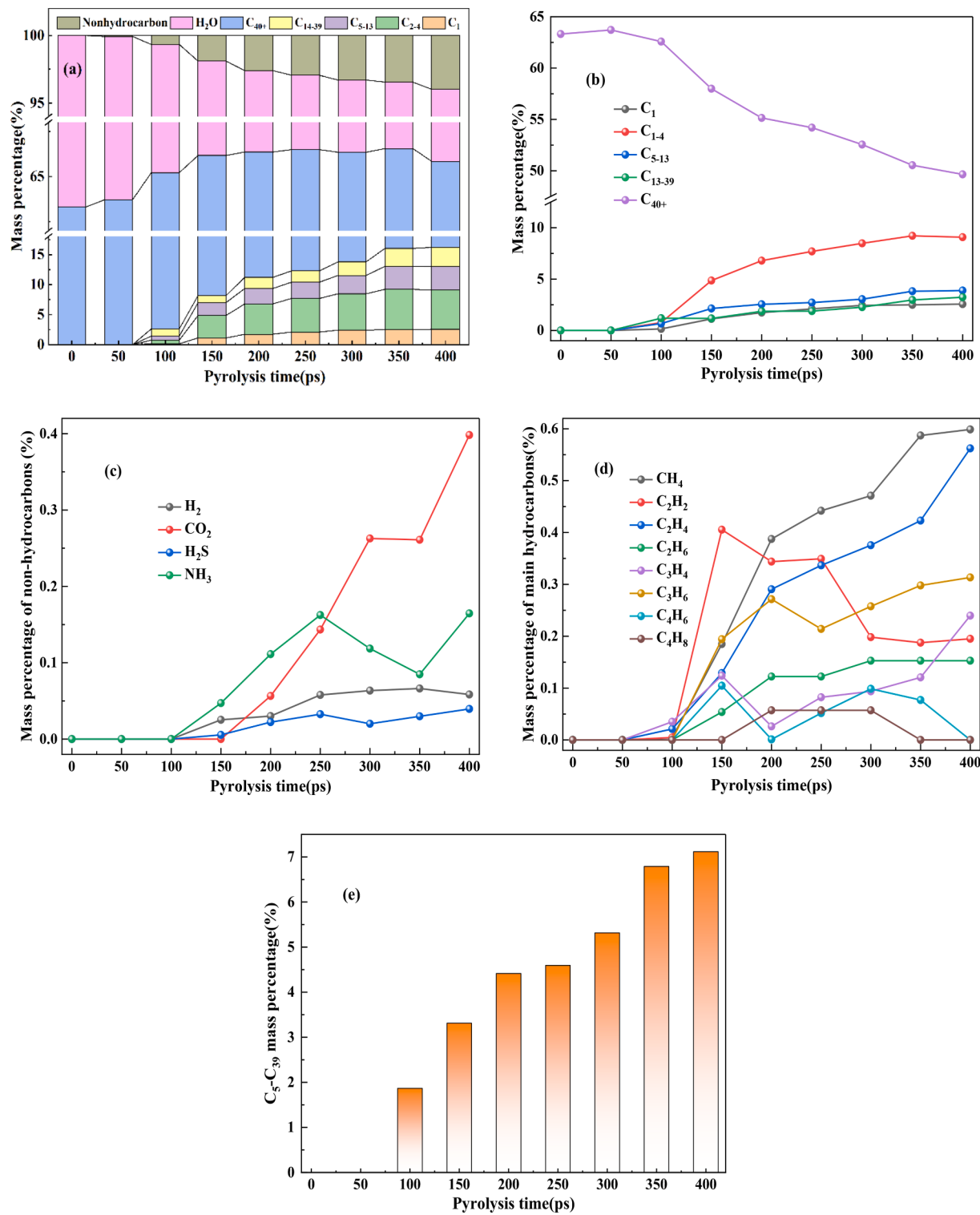


Fig. 8. Composition evolutions of pyrolysis products with the reaction time: (a) all pyrolysis products, (b) hydrocarbon products, (c) mainly non-hydrocarbon products, (d) gaseous hydrocarbon products and (e) liquid hydrocarbon products.

atoms. Then, the alkyl free radical loses or gets a hydrogen free radical, forming alkanes or alkenes. Here, the bond cleavage sites include any C–C bond or C–H bond in the aliphatic chain, C–C bonds, C–O bonds and C–S bonds connected to aromatic carbon atoms. At the same time, water molecules will break bonds to form [H] and [OH] radicals. Finally, the C–H bond on the aromatic carbon atom and the C–C bond connected to the aliphatic group cleave, forming [H] and aliphatic fragments, and the aromatic structure is further dehydrogenated and polymerized to form

coke.

The breaking of chemical bonds is generally carried out in accordance with the order of the bond energy but in a certain temperature range, several chemical bonds with slight difference in bond energy may cleave at the same time. Although the organic compounds produced by kerogen pyrolysis in the same temperature range are very complex, they are generally derived from the fracture of the same class covalent bonds with similar bond energies.

Table 1
Bond energy of the main chemical bonds in kerogen [46].

Number	Chemical bond	Bond energy KJ/mol	Smaller bond energies
1	C _{ar} -H	468.2–472.2	more benzene rings
2	C _{ar} -C _{ar}	478.6	—
3	C _{ar} -C _{al}	324–434.3	longer fat chain, more benzene rings
4	C _{ar} -O	313.8–332.2	—
5	C _{al} -S	318.0–327.6	more benzene rings
6	C _{al} -H	268.2–342.7	fewer benzene rings
7	C _{al} -C _{al}	247.3–319.7	more benzene rings in the fat chain
8	C _{al} -N	226.8–306.3	benzene ring <i>para</i> -substituents
9	C _{al} -O	155.0–309.2	aliphatic chain attached to the benzene ring, not to the branched chain
10	C _{al} -S	196.6–225.9	more benzene rings connected
11	C _{al} -N	123.0–218.4	connect the benzene ring, not the branch chain
12	S-S	184.1–230.0	fewer benzene rings connected
13	H-O-H	463	—

According to the analysis of pyrolysis simulation data and the statistics of chemical bond energy, the bond breaking sites of kerogen during pyrolysis is initially determined as shown in Fig. 9.

In the process of hydrocarbon generation during kerogen pyrolysis, the C_{al}-S bond and C_{ar}-C_{al}-O bond in the molecular structure of kerogen have relatively low bond energy, which thereby are easier to be broken in the early stage of the reaction (I in Fig. 9). Such cleaving processes could result in the formation of compounds including C₃H₅O and C₃H₅O₂. Besides, aliphatic carbon–carbon bonds, such as C_{al}-C_{al} bond and C_{al}-C_{al}-O bond, have strong reactivity. They will also break at the initial stage of reaction (II in Fig. 9), resulting in compounds including C₇H₁₁ and C₄H₈O. This simulation result is consistent with the results obtained by Zheng et al. [17] that aliphatic bridge bonds and alkyl ether bridge bonds are usually the first cleavage sites during the initial thermal decomposition process. The C_{ar}-C_{al} bonds in the macromolecular structure have a high bond energy, and they will be broken under the conditions of high temperature and long reaction time (III in Fig. 9) to generate benzene ring, C₄H₄NO and other compounds, which subsequently will react with [H] and [OH] generated by water decomposition.

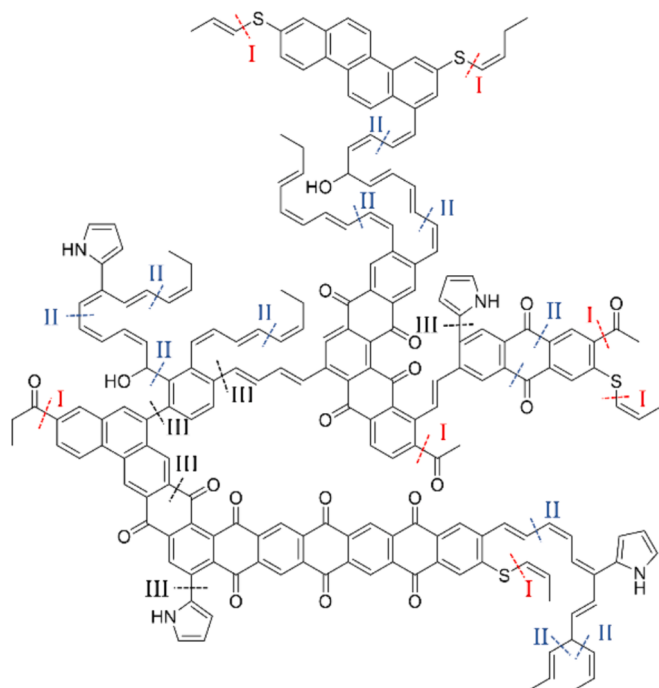


Fig. 9. Main reaction sites in kerogen pyrolysis reaction.

When the reaction temperature is high enough and the reaction time is long enough, Cal-H bond will break to generate a large number of small molecule pyrolysis products, such as H₂, C₂H₂, C₂H₆, etc.

3.4. Typical pathway of hydrocarbon generation

By observing the consumption and generation of H₂O in the reaction process, it can be found that water provides the necessary hydrogen source for kerogen in the reaction process, and promotes the pyrolysis reaction. In the process of hydrocarbon generation of overmature kerogen, the degree of dissociation of water gradually increases with the increase of reaction temperature, so that water has a larger ionic product constant, and the interaction between water, hydrocarbon and kerogen gradually increases, and the hydrocarbon generation reactions will more likely to occur. The molecular dynamics simulation of the reaction proved that water participated in the hydrocarbon generation not in the form of H₂, but in the form of [H] and [OH] generated by O–H bond fracture. The typical pathway of hydrocarbon generation in the presence of water is shown in Fig. 10.

In the presence of H₂O, the aliphatic branches of the carbonyl groups and the benzene rings were removed in the form of CO₂, H₂ and small hydrocarbon molecules. Then, the aliphatic chains connecting sulfur heteroatomic groups and benzene rings were broken to generate benzene rings, H₂S, etc. Subsequently, the benzene ring was further cracked to produce aliphatic hydrocarbons. Finally, the aliphatic hydrocarbons were cleaved to produce small molecules, such as alkanes and CH₄, etc.

3.5. Hydrocatalytic hydrocarbon generation model

The vitrinite reflectance of the Longmaxi shale kerogen is about 2.8 %, which belongs to the over-mature stage. Namely, the H/C ratio decreases sharply. According to the classical organic hydrocarbon generation model[3], the hydrocarbon generation potential of the Longmaxi shale kerogen has been nearly exhausted due to the restriction of hydrogen content in the kerogen base. Hydrogen content is the key factor restricting the hydrocarbon generation of high-over-mature kerogen.

Previous work has reported that H₂O was commonly discovered in different geological environments, and even several abnormal intervals containing H₂O and H₂ were found in ultra-deep environments at a depth of 6500 m. H₂O and H₂ in geological bodies may provide external hydrogen sources for the hydrocarbon generation process of overmature kerogen [35,48–50]. The presence of water medium has an important impact on the hydrocarbon generation process of organic matter, and different chemical properties of water medium will have different impacts on hydrocarbon generation products. The closed system pyrolysis experiment conducted by Lewan et al. [8] proved that type

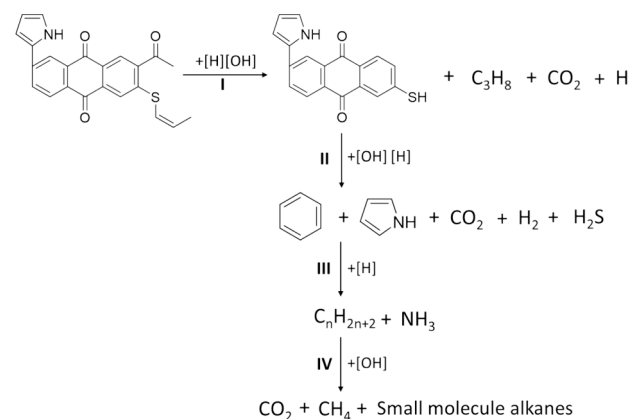


Fig. 10. Typical chemical reaction pathway of hydrocarbon generation evolution.

II kerogen generates more liquid hydrocarbons under the condition of water. Seewald et al. demonstrated that water could decompose and serve as hydrogen source during the hydrocarbons generation processes [51]. Helgeson et al. [52] assumed that the influence of water as a pressurizing medium on the hydrocarbon generation process may be related to the hydrolysis disproportionation reaction of organic matter.

The hydrocarbon generation by hydrolysis and disproportionation of organic matter is of economic and geological significance. The initial H/C ratio of kerogen does not accurately represent the final hydrocarbon generation potential of kerogen with the addition of external hydrogen sources. The hydrocarbon generation of kerogen in the deep environment under the presence of external hydrogen source may have a complex process involving activation, hydrocarbon generation, deactivation, and reactivation. In the deep basins, even though the H/C atomic ratio of kerogen is very low and traditional hydrocarbon generation models suggest there is almost no hydrocarbon potential, considerable late-stage gas can still be generated under high temperatures due to the presence of H_2O and H_2 [53].

Fig. 11 is the evolution model of deep-ultra deep multi-pathway hydrocarbon generation. According to traditional model by Tissot et al. [9,34], the organic matter of source rocks could generate a large amount of oil and gas (equivalent to $Ro \approx 1.2 \sim 2.0\%$) in the mature evolution stage, and the hydrocarbon generation termination threshold was at $Ro = 2.0\%$. When Ro exceeded 2.0% , the natural gas generated was mainly CH_4 from kerogen cracking until the gas generation termination threshold was reached at $Ro = 3.0\%$ on the basis of kerogen cracking model [54]. Pang et al. [55] have determined the active source rock depth limit (ASDL) of 6 representative petroleum basins using the material balance method. The measured results showed that the ASDL of

basins around the world ranged from 3,000 to 16,000 m, and the thermal maturity (Ro) of source rocks at ASDL was almost around $Ro \approx 3.5 \pm 0.5\%$, indicating that the hydrocarbon gas death line of source rocks was $3.5 \pm 0.5\% Ro$.

Jia and Zhang believed that ultra-deep buried environment, high temperature and complex fluid conditions leaded to the complex and diverse hydrocarbon genesis. In addition to hydrocarbon generation by thermal evolution of organic matter, there was also secondary cracking of crude oil generated in early stage [5]. Such multiple gas generation model leaded to the downward movement of hydrocarbon generation death line. The organic-inorganic hydrogenation gas could extend the hydrocarbon generation death line to $Ro = 3.5\%$, indicating that the gas death line of kerogen could be continuously lowered if sufficient hydrogen source was provided in the hydrocarbon generation reaction process. In this study, an over-mature kerogen with a vitrinite reflectance of 2.8 % was selected. Under the hydrogen-supplying conditions with water, the kerogen still exhibited significant hydrocarbon generation potential with the conversion rate of kerogen hydrocarbon generation gas up to 22.28 %. The research results validate the hydrogen addition hydrocarbon generation mechanism and pathways. Theoretically, continuous hydrogen addition can reactivate the over-mature kerogen to generate hydrocarbon, thereby lowering the hydrocarbon generation termination threshold.

4. Conclusions

In summary, the reaction molecular dynamics simulation has been conducted based on true molecular structure model established from the shale kerogen of Longmaxi Formation, Sichuan Basin. The simulation

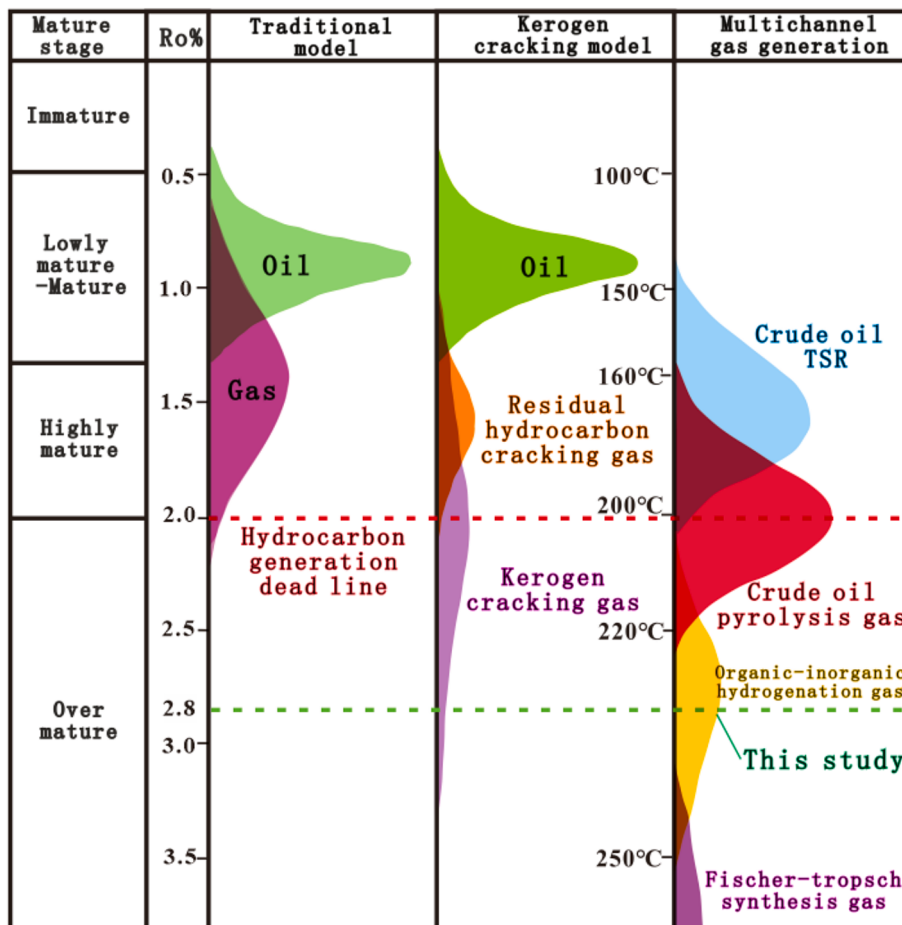


Fig. 11. Evolution model of deep-ultra deep multi-pathway hydrocarbon generation [5,9].

results demonstrated that over-mature kerogens with Ro 2.8 % could continue to transform to hydrocarbon with the hydrogen supply from H₂O. Meanwhile, the total rate of hydrocarbon generation could reach up to 22.28 %, which could break through the hydrocarbon generation dead line of traditional hydrocarbon generation models.

During the hydrogenation catalysis reaction process, similar to classical hydrocarbon generation, temperature and reaction time are the main factors affecting hydrocarbon production via pyrolysis of kerogen. Both natural gas and shale oil production were increasing as reaction temperature rises. As the temperature increased to 2500 K, natural gas production continuously increased while the content of heavy shale oil decreased because of secondary cracking. This indicated that high temperature was conducive to the generation of natural gas, and low temperature was favorable to the formation of larger molecules. Extending the reaction time had a phased positive effect on the products. At the initial stage of the reaction, increasing the reaction time by 1 time could significantly promote the generation of oil and gas productions by 3.65 times. Further increasing reaction time by 1 time has a relatively minor impact on oil and gas productions by 0.45 times.

The molecular simulation of kerogen pyrolysis showed that the number and types of reaction products at high temperature were more than those at low temperature. Small molecules such as free radicals initially generated by the reaction participated in the subsequent reaction, aiding in the decomposition processes of the macromolecule into small molecules. During the pyrolysis process of kerogen molecules, the Cal-S bond, Car-Cal-O bond, Cal-Cal bond, Cal-Cal-O bond, Car-Cal bond and Cal-H bond were broken in sequence according to the bond energy. The cleavage of various chemical bonds in macromolecules was intersectional, and several bonds with similar chemical bond energy may react at the same time. Kerogen molecular compounds have a special hydrolytic disproportionation pathway for hydrocarbon generation in the presence of H₂O. This is the underlying cause for over-mature kerogens being activated to continuously generate hydrocarbon generation with the hydrogen supply.

CRediT authorship contribution statement

Guili Ma: Writing – review & editing, Writing – original draft, Resources, Methodology, Conceptualization. **Junqing Chen:** Writing – review & editing, Writing – original draft, Resources. **Changtao Yue:** Writing – review & editing, Validation, Investigation, Data curation. **Yue Ma:** Writing – review & editing, Writing – original draft, Methodology, Formal analysis, Data curation, Conceptualization. **Lu Gong:** Project administration, Methodology, Funding acquisition. **Yuying Wang:** Visualization, Software, Methodology. **Fujie Jiang:** Funding acquisition, Formal analysis, Data curation, Conceptualization. **Hong Pang:** Writing – review & editing, Writing – original draft, Methodology, Conceptualization. **Xinyi Niu:** Visualization, Validation, Software.

Declaration of competing interest

The authors declare that they have no known competing financial interests or personal relationships that could have appeared to influence the work reported in this paper.

Data availability

No data was used for the research described in the article.

Acknowledgements

This work was supported by the National Natural Science Foundation of China (No. 42102145), the Science Foundation of China University of Petroleum, Beijing (No. 2462022YXZZ007).

References

- [1] Yang Z, Zou CN, Wu ST, Lin SH, Pan SQ, Niu XB, et al. Formation, distribution and resource potential of the “sweet areas (sections)” of continental shale oil in China. *Mar Pet Geol* 2019;102:48–60. <https://doi.org/10.1016/j.marpetgeo.2018.11.049>.
- [2] Zhao WZ, Hu SY, Hou LH, Yang T, Li X, Guo BC, et al. Types and resource potential of continental shale oil in China and its boundary with tight oil. *Pet Explor Dev* 2020;47(1):1–11. [https://doi.org/10.1016/S1876-3804\(20\)60001-5](https://doi.org/10.1016/S1876-3804(20)60001-5).
- [3] Wang EZ, Guo TL, Li MW, Li CR, Dong XX, Zhang NX, et al. Exploration potential of different lithofacies of deep marine shale gas systems: Insight into organic matter accumulation and pore formation mechanisms. *J Nat Gas Sci Eng* 2022;102:104563. <https://doi.org/10.1016/j.jngse.2022.104563>.
- [4] He DF, Jia CZ, Zhao WZ, Xu FY, Luo XR, Liu WH, et al. Research progress and key issues of ultra-deep oil and gas exploration in China. *Pet Explor Dev* 2023;50(6):1133–44. [https://doi.org/10.1016/S1876-3804\(24\)60470-2](https://doi.org/10.1016/S1876-3804(24)60470-2).
- [5] Jia CZ, Zhang SC. The formation of marine ultra-deep petroleum in China. *Acta Geol Sin* 2023;97(9):2775–801. <https://doi.org/10.19762/j.cnki.dzixuebaobao.2023201>.
- [6] Jia CZ. Breakthrough and significance of unconventional oil and gas to classical petroleum geology theory. *Pet Explor Dev* 2017;44(1):1–10. [https://doi.org/10.1016/S1876-3804\(17\)30002-2](https://doi.org/10.1016/S1876-3804(17)30002-2).
- [7] Wu YD, Ji LM, He C, Zhang ZN, Zhang MZ, Sun LN, et al. The effects of pressure and hydrocarbon expulsion on hydrocarbon generation during hydrous pyrolysis of type-I kerogen in source rock. *Gas Sci Eng* 2016;34:1215–24. <https://doi.org/10.1016/j.jngse.2016.08.017>.
- [8] Lewan MD, Roy S. Role of water in hydrocarbon generation from type I kerogen in Mahogany oil shale of the Green River Formation. *Org Geochem* 2011;42(1):31–41. <https://doi.org/10.1016/j.orggeochem.2010.10.004>.
- [9] Tissot BP, Welte DH. *Petroleum formation and occurrence*. New York: Springer Verlag; 1984.
- [10] Landais P, Michels R, Elie M. Are time and temperature the only constraints to the simulation of organic matter maturation? *Org Geochem* 1994;22(3–5):617–30. [https://doi.org/10.1016/0146-6380\(94\)90128-7](https://doi.org/10.1016/0146-6380(94)90128-7).
- [11] Fang CH, Li SY, Ma GL, Wang HY, Huang ZL. Reaction mechanism and Kinetics of pressurized pyrolysis of Chinese oil shale in the presence of water. *Pet Sci* 2012;9:532–4. <https://doi.org/10.1007/s12182-012-0239-0>.
- [12] Li QY, Han XX, Liu QQ, Jiang XM. Thermal decomposition of Huadian oil shale. Part 1. Critical organic intermediates. *Fuel* 2014;121 (2):109–16. Doi: 10.1016/j.fuel.2013.12.046.
- [13] Huang YR, Han XX, Jiang XM. Comparison of fast pyrolysis characteristics of Huadian oil shales from different mines using Curie-point pyrolysis–GC/MS. *Fuel Process Technol* 2014;128:456–60. <https://doi.org/10.1016/j.fuproc.2014.08.007>.
- [14] Yan LJ, Bai YH, Zhao RF, Li F, Xie KC. Correlation between coal structure and release of the two organic compounds during pyrolysis. *Fuel* 2015;145(1):12–7. <https://doi.org/10.1016/j.fuel.2014.12.056>.
- [15] Gao MJ, Li XX, Guo L. Pyrolysis simulations of Fugu coal by large-scale ReaxFF molecular dynamics. *Fuel Process Technol* 2018;178:197–205. <https://doi.org/10.1016/j.fuproc.2018.05.011>.
- [16] Hong DK, Guo X. Molecular dynamics simulations of Zhundong coal pyrolysis using reactive force field. *Fuel* 2017;210:58–66. <https://doi.org/10.1016/j.fuel.2017.08.061>.
- [17] Zheng M, Li XX, Nie FG, Guo L. Investigation of overall pyrolysis stages for Liulin bituminous coal by large-scale ReaxFF molecular dynamics. *Energy Fuel* 2017;31(4):3675–83. <https://doi.org/10.1021/acs.energyfuels.6b03243>.
- [18] Wang K, Zhang H, Wang X, Fan WD. Study on pyrolysis mechanism of coal in hydrogen-rich atmosphere based on reactive molecular dynamics simulation. *Int J Hydrogen Energy* 2024; 49(D):861–72. Doi: 10.1016/j.ijhydene.2023.08.060.
- [19] Bhoi S, Banerjee T, Mohanty K. Insights on the combustion and pyrolysis behavior of three different ranks of coals using reactive molecular dynamics simulation. *RSC Adv* 2016;6(4):2559–70. <https://doi.org/10.1039/C5RA23181G>.
- [20] Li XX, Zheng M, Ren CX, Guo L. ReaxFF Molecular dynamics simulations of thermal reactivity of various fuels in pyrolysis and combustion. *Energy Fuel* 2021;35(15):11707–39. <https://doi.org/10.1021/acs.energyfuels.1c01266>.
- [21] Zheng M, Li XX, Liu J, Guo L. Initial chemical reaction simulation of coal pyrolysis via ReaxFF molecular dynamics. *Energy Fuel* 2013;27(6):2942–51. <https://doi.org/10.1021/ef400143z>.
- [22] Zhan JH, Wu R, Liu X, Gao SQ, Xu GW. Preliminary understanding of initial reaction process for subbituminous coal pyrolysis with molecular dynamics simulation. *Fuel* 2014;134:283–92. <https://doi.org/10.1016/j.fuel.2014.06.005>.
- [23] Liang YH, Wang F, Zhang H, Wang JP, Li YY, Li GY. A ReaxFF molecular dynamics study on the mechanism of organic sulfur transformation in the hydropyrolysis process of lignite. *Fuel Process Technol* 2016;147:32–40. <https://doi.org/10.1016/j.fuproc.2015.09.007>.
- [24] Li YY, Li GY, Zhang H, Wang JP, Li AQ, Liang YH. ReaxFF study on nitrogen-transfer mechanism in the oxidation process of lignite. *Fuel* 2017;193:331–42. <https://doi.org/10.1016/j.fuel.2016.12.081>.
- [25] Liu XP, Zhan JH, Lai DG, Liu XX, Zhang ZJ, Xu GW. Initial pyrolysis mechanism of oil shale kerogen with reactive molecular dynamics simulation. *Energy Fuel* 2015;29(5):2987–97. <https://doi.org/10.1021/acs.energyfuels.5b00084>.
- [26] Qian YN, Zhan JH, Lai DG, Li MY, Liu XX, Xu GW. Primary understanding of non-isothermal pyrolysis behavior for oil shale Kerogen using reactive molecular dynamics simulation. *Int J Hydrogen Energy* 2016;41(28):12093–100. <https://doi.org/10.1016/j.ijhydene.2016.05.106>.
- [27] Zhong QF, Mao QY, Xiao J, van Duin ACT, Mathews JP. ReaxFF simulations of petroleum coke sulfur removal mechanisms during pyrolysis and combustion.

- Combust Flame 2018;198:146–57. <https://doi.org/10.1016/j.combustflame.2018.09.005>.
- [28] Zhang ZJ, Chai J, Zhang HY, Guo LT, Zhan JH. Structural model of LongKou oil shale Kerogen and the evolution process under steam pyrolysis based on ReaxFF molecular dynamics simulation. Energy Source 2019;43(2):252–65. <https://doi.org/10.1080/15567036.2019.1624879>.
- [29] Han QY, Li MJ, Liu XQ, Xiao H, Ren JH, Guo CB. A maturation scale for molecular simulation of Kerogen thermal degradation. Org Geochem 2023;175:104507. <https://doi.org/10.1016/j.orggeochem.2022.104507>.
- [30] Shi KY, Chen JQ, Pang XQ, Jiang FJ, Hui SS, Zhang SJ, et al. Average molecular structure model of shale Kerogen: Experimental characterization, structural reconstruction, and pyrolysis analysis. Fuel 2024;355:129474. <https://doi.org/10.1016/j.fuel.2023.129474>.
- [31] Zhang ZJ, Guo LT, Zhang HY, Zhan JH. Comparing product distribution and desulfurization during direct pyrolysis and hydropyrolysis of Longkou oil shale kerogen using reactive MD simulations. Int J Hydrogen Energy 2019; 44(47): 25335–46. Doi: 10.1016/j.ijhydene.2019.08.036.
- [32] Zhao FM, Li B, Zhang L, Che DC, Liu SY. The mechanism of superheated steam affecting the quality of in-situ pyrolyses of oil shale kerogen: Part A-saturation of pyrolytic organics. Fuel 2022;323:124331. <https://doi.org/10.1016/j.fuel.2022.124331>.
- [33] Tong JH, Jiang XM, Han XX, Wang XY. Evaluation of the macromolecular structure of Huadian oil shale Kerogen using molecular modeling. Fuel 2016;181:330–9. <https://doi.org/10.1016/j.fuel.2016.04.139>.
- [34] Tissot B, Durand B, Espitalie J, Combaz A. Influence of nature and diagenesis of organic matter in formation of petroleum. AAPG Bull 1974;58(3):499–506. <https://doi.org/10.1306/83d91425-16c7-11d7-8645000102c1865d>.
- [35] Seewald JS. Organic–inorganic interactions in petroleum-producing sedimentary basins. Nature 2003;426:327–33. <https://doi.org/10.1038/nature02132>.
- [36] Zhao WZ, Zhang SC, He K, Zeng HL, Hu GY, Zhang B, et al. Origin of conventional and shale gas in Sinian lower Paleozoic strata in the Sichuan basin: Relayed gas generation from liquid hydrocarbon cracking. AAPG Bull 2019;103(6):1265–96. <https://doi.org/10.1306/11151817334>.
- [37] Liu XJ, Luo DX, Xiong J, Liang LX. Construction of the average molecular modeling of the kerogen from the Longmaxi formation. Chem Industry Eng Progr 2017;36 (2):530–57. <https://doi.org/10.16085/j.issn.1000-6613.2017.02.019>.
- [38] van Duin ACT, Dasgupta S, Lorant F, Goddard WA. ReaxFF: a reactive force field for hydrocarbons. Chem A Eur J 2001;105(41):9396–409. <https://doi.org/10.1021/jp004368u>.
- [39] Lewan MD. Laboratory simulation of petroleum formation hydrous pyrolysis. Org Geochem 1993;18:419–42. <https://doi.org/10.1007/978-1-4615-2890-6-18>.
- [40] Behar F, Lewan MD, Lorant F, Vandebroucke M. Comparison of artificial maturation of lignite in hydrous and nonhydrous conditions. Org Geochem 2003; 34(4):575–600. [https://doi.org/10.1016/S0146-6380\(02\)00241-3](https://doi.org/10.1016/S0146-6380(02)00241-3).
- [41] Li GY, Li AQ, Zhang H, Wang JP, Chen SY, Liang YH. Theoretical study of the CO formation mechanism in the CO₂ gasification of lignite. Fuel 2018;211:353–62. <https://doi.org/10.1016/j.fuel.2017.09.030>.
- [42] Zhou Q, Zou T, Zhong M, Zhang YM, Wu RC, Gao SQ, et al. Lignite upgrading by multi-stage fluidized bed pyrolysis. Fuel Process Technol 2013;116:35–43. <https://doi.org/10.1016/j.fuproc.2013.04.022>.
- [43] Guan XH, Wang D, Wang Q, Chi MS, Liu CG. Estimation of various chemical bond dissociation enthalpies of large-sized kerogen molecules using DFT methods. Mol Phys 2016;114(11):1705–55. <https://doi.org/10.1080/00268976.2016.1143983>.
- [44] Döntgen M, Przybylski-freund MD, Kröger LC, Kopp WA, Ismail AE, Leonhard K. Automated discovery of reaction pathways, rate constants, and transition states using reactive molecular dynamics simulations. J Chem Theory Comput 2015; 11 (6): 2517–24. Doi: 10.1021/acs.jctc.5b00201.
- [45] Morgan TJ, Kandiyoti R. Pyrolysis of Coals and Biomass: Analysis of Thermal Breakdown and Its Products. Chem Rev 2014;114(3):1547–607. <https://doi.org/10.1021/cr400194p>.
- [46] Shi L, Liu QY, Guo XJ, Wu WZ, Liu ZY. Pyrolysis behavior and bonding information of coal-A TGA study. Fuel Process Technol 2013;108:125–32. <https://doi.org/10.1016/j.fuproc.2012.06.023>.
- [47] Shi L, Liu QY, Zhou B, Guo XJ, Li ZK, Cheng XJ, et al. Understanding the evolution of methane and hydrogen in coals pyrolysis in a view point of bond cleavage. Energy Fuel 2017;31(1):429–37. <https://doi.org/10.1021/acs.energyfuels.6b02482>.
- [48] Yang YN, Zhong NN, Wu J, Pan YY. Deep-basin gas generation via organic–inorganic interactions: New insights from redox-controlled hydrothermal experiments at elevated temperature. Int J Coal Geol 2022;257:104009. <https://doi.org/10.1016/j.coal.2022.104009>.
- [49] Simoneit BRT. Petroleum generation, an easy and widespread process in hydrothermal systems: an overview. Appl Geochem 1990;5(1–2):3–15. [https://doi.org/10.1016/0883-2927\(90\)90031-y](https://doi.org/10.1016/0883-2927(90)90031-y).
- [50] Zgonnik V. The occurrence and geoscience of natural hydrogen: A comprehensive review. Earth Sci Rev 2020;203:103140. <https://doi.org/10.1016/j.earscirev.2020.103140>.
- [51] Seewald JS, Eglington LB, Ong YL. An experimental study of organic–inorganic interactions during vitrinite maturation. Geochim Cosmochim Acta 2000;64(9): 1577–91. [https://doi.org/10.1016/S0016-7037\(00\)00339-2](https://doi.org/10.1016/S0016-7037(00)00339-2).
- [52] Helgeson HC, Knox AM, Owens CE, Shock EL. Petroleum, oil field waters, and authigenic mineral assemblages: Are they in metastable equilibrium in hydrocarbon reservoirs. Geochim Cosmochim Acta 1993;57(14):3295–339. [https://doi.org/10.1016/0016-7037\(93\)90541-4](https://doi.org/10.1016/0016-7037(93)90541-4).
- [53] Price LC. Metamorphic free-for-all. Nature 1994;370(6487):253–4. <https://doi.org/10.1038/370253a0>.
- [54] Chen JP, Zhao WZ, Xiao ZY, Zhang SC, Deng CP, Sun YG, et al. A discussion on the upper limit of maturity for gas generation by marine kerogens and the utmost of gas generative potential: Taking the study on the Tarim Basin as an example. Sci Bull 2007;52:125–32. <https://doi.org/10.1007/s11434-007-6015-7>.
- [55] Pang XQ, Jia CZ, Zhang K, Li MW, Wang YW, Peng JW, et al. The dead line for oil and gas and implication for fossil resource prediction. Earth Syst Sci Data 2020;12: 577–90. <https://doi.org/10.5194/essd-12-577-2020>.